

Article

A Novel Layout for Combined Heat and Power Production for a Hospital Based on a Solid Oxide Fuel Cell [†]

Francesco Calise , Francesco Liberato Cappiello * , Luca Cimmino , Massimo Dentice d'Accadia 
and Maria Vicidomini

Department of Industrial Engineering, Università Degli Studi "Federico II", 80124 Napoli, Italy; frcalise@unina.it (F.C.); luca.cimmino@unina.it (L.C.); dentice@unina.it (M.D.d.); maria.vicidomini@unina.it (M.V.)

* Correspondence: francescoliberato.cappiello@unina.it

[†] The present paper is an extension of the conference paper presented to the conference ECOS 2023.

Abstract: This paper addresses the problem of the reduction in the huge energy demand of hospitals and health care facilities. The sharp increase in the natural gas price, due to the Ukrainian–Russian war, has significantly reduced economic savings achieved by combined heat and power (CHP) units, especially for hospitals. In this framework, this research proposes a novel system based on the integration of a reversible CHP solid oxide fuel cell (SOFC) and a photovoltaic field (PV). The PV power is mainly used for balancing the hospital load. The excess power production is exploited to produce renewable hydrogen. The SOFC operates in electrical tracking mode. The cogenerative heat produced by the SOFC is exploited to partially meet the thermal load of the hospital. The SOFC is driven by the renewable hydrogen produced by the plant. When this hydrogen is not available, the SOFC is driven by natural gas. In fact, the SOFC is coupled with an external reformer. The simulation model of the whole plant, including the reversible SOFC, PV, and hospital, is developed in the TRNSYS18 environment and MATLAB. The model of the hospital is calibrated by means of measured data. The proposed system achieves very interesting results, with a primary energy-saving index of 33% and a payback period of 6.7 years. Therefore, this energy measure results in a promising solution for reducing the environmental impact of hospital and health care facilities.



Citation: Calise, F.; Cappiello, F.L.; Cimmino, L.; Dentice d'Accadia, M.; Vicidomini, M. A Novel Layout for Combined Heat and Power Production for a Hospital Based on a Solid Oxide Fuel Cell. *Energies* **2024**, *17*, 979. <https://doi.org/10.3390/en17050979>

Academic Editor: Adam Smoliński

Received: 26 December 2023

Revised: 5 February 2024

Accepted: 16 February 2024

Published: 20 February 2024



Copyright: © 2024 by the authors. Licensee MDPI, Basel, Switzerland. This article is an open access article distributed under the terms and conditions of the Creative Commons Attribution (CC BY) license (<https://creativecommons.org/licenses/by/4.0/>).

Keywords: combined heat and power production; solid oxide fuel cell; renewable hydrogen; photovoltaic; electric energy storage; energy storage; energy savings for hospital; health care facilities

1. Introduction

Over the past few decades, buildings have been one of the key sectors responsible for high energy demands (36%) [1]. This sector has also resulted in being one of the major contributors to humans' environmental footprint; therefore, this sector must play a pivotal role in the transition [2]. In this framework, hospitals and health care facilities (HHF) play a critical role [3]. In fact, they must guarantee a 24/7 service, with a huge electric and thermal energy demand [4]. Studies reveal that hospitals use about 6% of the whole energy consumption in this sector [5]. Due to their continuous and complex operation requirements, HHF are energy-intensive, and therefore they have significant operating costs and high environmental impacts [6]. A typical energy profile in HHF presents intermittent and continuous load operation, resulting in energy consumption per square foot twice that of office buildings [7].

Several works available in the literature try to face the issue of the high energy consumption of HHF [8–10]. Common energy measures regard the refurbishment of the building envelope [11] and advanced technologies for the heat ventilation and conditioning system (HVAC) [12]. Energy efficiency is also crucial in order to reduce the overall primary energy demand. In this framework, the selection of suitable building orientations, lighting

efficiency, window-to-wall ratios, and insulation materials is crucial to reducing energy consumption, total costs, and CO₂ emissions [13]. Recently, power-to-gas technology has been progressively identified as an economically and technically feasible method for compensating the unbalanced hospital-oriented supply network [14]. Moreover, given such large energy consumption and the simultaneity of electric and thermal loads, energy measures based on cogeneration of heat and power (CHP) and trigeneration of cool, heat, and power (CCHP) are widely adopted, leading to significant economic and energy savings [15,16]. Moreover, these technologies are mature, reliable, and widely commercially adopted [17,18]. The adoption of a CHP reciprocating combustion engine is proven to achieve a significant reduction in primary energy consumption and operating costs [19,20]. In the framework of this study of the integration of CHP and HFF, Calise et al. [19] proposed several CHP reciprocating combustion engine layouts and several control strategies to find out which solution better fits the energy needs of a large hospital located in Stuttgart, Germany. In particular, three configurations are considered: (i) a single combined heat and power reciprocating engine; (ii) two combined heat and power reciprocating engines; and (iii) one combined heat and power reciprocating engine coupled with a photovoltaic (PV) field. Two novel hybrid control strategies are proposed: master electric load-slave electric load and master thermal load-slave electric load. By means of dynamic simulations carried out in a TRNSYS 18 environment, the work assesses that the third layout exhibits better energy and environmental performances, achieving a simple payback (SPB) of 1.6 years. Alexis et al. [21] assess that the installation of CHP serving a hospital located in Greece reduces the primary energy consumption of the hospital by 28%, while at the same time achieving a reduction in the yearly operative costs by 32%.

Gimelli and Muccillo [22] analyzed the integration of CHP and HFF, assessing that internal combustion engines operating in a cogeneration mode are able to reduce energy consumption by up to 19%, deeply depending on the load profiles of the user. Ghoreishinejad et al. [23] performed a multi-objective optimization of a CCHP system based on heat recovery from an oxygen generator for a hospital building in Sabzevar city. This system includes an ORC component, an absorption chiller cycle, air handlers, and heat exchangers. The plant is able to supply a certain amount of the electricity, heating, cooling, and hot water needs of this hospital during different seasons of the year based on three scenarios. The system was analyzed from an energy, exergy, and economic point of view. According to the findings, this project can act as a facilitator in hospitals with a minimum of three oxygen generators. A novel concept of hospital-oriented quad-generation (HOQG) to produce a combined cooling, heating, power, and gas (CCHPG) system is investigated by Chen et al. [24]. The proposed plant includes a PV field and wind turbines, a high-temperature superconducting (HTS) power cable, and superconducting magnetic energy storage (SMES). The plant simultaneously produces multiple clean energies and medical gases (oxygen, nitrogen, and carbon dioxide) during both normal and emergency operations. Compared to conventional copper cable and electrochemical batteries, HTS terminal power units result in high-efficiency power delivery and high-quality power compensation. Three cryogenic fluids of liquefied methane gas, liquefied oxygen, and liquefied nitrogen are used as backups for both energy fuel and medical gas. For the 10 MW hospital building case, the proposed plant can save approximately 10.63 GWh of electricity per year. Calise et al. [25] modeled the dynamic energy performance of a hospital integrated with a CHP reciprocating engine. The selected hospital is located in Puglia (south of Italy) and has a capacity of roughly 600 beds. The hospital simulation model is developed in TRNSYS. Although the results show that the primary energy saving (PES) is limited (about 9%), the plant shows very good economic results, with an SPB of 1.5 years and a net present value (NPV) of EUR 7.10 M.

However, the Ukrainian war, which started in 2022, has caused a relevant increase in the natural gas price in Europe in the last year [26,27]. This makes the CHP plant operation extremely expensive, dramatically affecting the energy bill of HFF. It is well known that the price of natural gas is dramatically dependent on the present geopolitical scenario

due to the limitations connected to the gas distribution infrastructure [28]. The European Union imports the majority of natural gas, used for a plurality of applications (electricity production, heat, industrial users, etc.). This represents a huge vulnerability for the energy security of the EU [29]. Therefore, the recent energy policies in the EU aim to dramatically reduce the importation of natural gas while also promoting the electrification of final user demand [30,31]. An interesting solution in this framework may be the integration of green hydrogen—obtained by converting renewable electricity—and reversible fuel cells. In this case, the surplus of renewable energy is used to produce green hydrogen [32], which is delivered to the fuel cell when the renewable energy source is not available [33]. Hydrogen fuel cells have been widely recognized for their cleanliness, efficiency, and flexibility, and their conversion characteristics from hydrogen to electricity and heat enable them to connect various energy components [34].

In this framework, one of the most promising technologies for electrolysis and electricity production from hydrogen is the reversible solid oxide fuel cell (r-SOFC) [35]. The r-SOFC is characterized by high installation and management costs due to its high operating temperature. It operates at about 500–800 °C. Therefore, specific materials must be used to manufacture this device [36]. On the other hand, this offers the possibility to exploit waste heat at high temperatures, configuring it as a promising CHP system [37]. A new paradigm for residential energy storage is proposed by Calise et al. [38]. The presented system is based on a PV field of 100 kW coupled with an r-SOFC, which produces hydrogen by exploiting the surplus of PV power. The hydrogen is stored in a pressurized tank with a maximum pressure of 200 bar. The results show that the system leads to a PES of roughly 60%, but it exhibits low economic profitability, i.e., a payback period of 15 years, due to the remarkably high capital cost of the plant. Also, Sun et al. [39] presented the optimal energy scheduling for a fuel cell-based cogeneration system for a residential application. The studied cogeneration system consists of a fuel cell, a PV field, a heat pump, and electric and thermal energy storages. They developed an economic optimization scheduling model assuming the minimum hydrogen consumption of a fuel cell in its full 24 h operation as an objective function and considering the balance of supply and demand and security constraints of the devices. To convert the randomness to the probability of the random variables, including PV and electrical and thermal power, we used the time-varying Markov chains. The results of the numerical simulation show that the fuel cell works securely with a maximum power not surpassing 2.5 kW. The hydrogen consumption by fuel cell power generation is 0.994 kg. The coupling of storage based on metal hydride hydrogen technology with a fuel cell in order to increase the system's energy efficiency is investigated in the work of Boghilla et al. [40]. In this work, metal hydride hydrogen storage and the reversible fuel cell are coupled with a vapor absorption refrigeration system for hydrogen storage and cooling applications simultaneously. In the fuel cell mode, the resulting system efficiencies with and without the vapor absorption refrigeration system at 80 °C were 73.29% and 47.84%, respectively. In the electrolyzer mode, the achieved maximum efficiency is 85.65%. With the use of metal hydride hydrogen storage, the overall efficiency of the electrolyzer increased to 94.05%.

In the framework of the integration of HHF and fuel cells, Tariq [41] proved the profitability of the adoption of a PV field together with an electrolyzer and a fuel cell for HHF. In this case, the adopted plant is mainly designed to match the hospital's electricity and oxygen demand. In particular, this research considered a power plant based on a PEM electrolyzer, a PEM fuel cell, and a PV field serving a typical Pakistani hospital. The author carried out several analyses for different Pakistani weather zones using Homer Pro software. This research assessed the good profitability of such a plant, proving a levelized cost of energy of 0.32 USD/kWh. However, this study does not take into account the thermal energy demand of the hospital, focusing only on the oxygen and power demands.

In the framework of the integration of HHF and fuel cell-based CHP, Isa et al. [42] proposed a cogeneration system consisting of a grid-connected PV (120 kW), a 100 kW proton exchange membrane fuel cell (PEMFC), and a battery and serving the University

Kebangsaan Malaysia Medical Centre, an educational hospital, since 1997. The system also includes a steam methane reformer, which allows the cell to operate using natural gas. The PEMFC and the PV field are able to meet the power load of the hospital. The waste heat from the fuel cell is used for driving heat recovery boilers and sterilizing equipment in the hospital. The techno-economic analysis is performed by means of the HOMER simulation software. The results show that the proposed system can reduce system costs by 30% with a profit index of 1.30. Despite the high capital costs, the proposed system is able to achieve these profitable economic results thanks to the incentives provided by the Malaysian Government for renewables and high energy efficiency technologies. A novel hospital-oriented combined cooling, heating, power, and oxygen (CCHPO) system is presented in the work of Zhan et al. [43]. The system is designed to guarantee the simultaneous supply of clean energies and medical gas during normal and emergency operations. The plant first consumes the excess photovoltaic power to produce hydrogen and oxygen by electrolysis, and then it stores the liquefied methane gas and liquefied oxygen by means of methanation and refrigeration. In emergency situations, the CCHPO system rapidly gasifies the stored liquefied methane gas into the local combined-cycle power plants for hospital power generation and further uses the waste heat to produce extra cooling and/or heating supplies. In a realistic hospital case study of China, the annual greenhouse gas emission reduction can be up to 4438.4 tons. Sleiti et al. [44] propose an energy, economic, and environmental analysis of a CHP power plant based on a solid oxide fuel cell. This system is designed to serve the National Center for Cancer Care and Research in Qatar, and it is based on measured and real energy and geometric data. The hydrogen to be delivered to the cell is produced by means of an internal steam methane reformer. The heat produced by the electrochemical reaction is partially used to meet the thermal energy needed for the internal reform of the methane. The residual amount of thermal energy is exploited for the cooling and heating systems. The results of the simulation show that the SOFC-CCHP system can save about 49% to 77% of the monthly bill of the hospital compared with the baseline system with an SPB of 10 years. In addition, the system leads to an equivalent CO₂ emission saving of 88% compared with the baseline system. The main limitation of this work is that the proposed model is based on a stationary approach, not paying attention to the dynamic evolution of the boundary conditions and the user load. Ghimire et al. [45] proposed a cogeneration plant based on a PEM fuel cell designed for operating as a backup system in a hospital located in Nepal. This study proved that a PEM fuel cell can be considered a valuable alternative to a conventional diesel generator backup system. The main limitation of this study relies on the fact that this paper is mainly focused on the yearly economic performance without providing a detailed dynamical analysis of the performance of the proposed system.

Aim of the Paper

The aim of the present work is to replace the conventional reciprocating engine producing heating, cooling, and electric energy with an innovative r-SOFC-based CCHP system coupled with a PV field. This energy measure is designed to increase the share of renewables in the hospital and reduce the consumption of natural gas without affecting the reliability and continuity of energy dispatch ensured by CHP-based technologies. The case study is the hospital “Miulli”, located in Puglia, south of Italy. In particular, the electric load of the hospital is primarily matched by the PV field and secondarily by the SOFC. The excess renewable power is supplied to the r-SOFC operating in electrolysis mode to produce hydrogen, which is stored in a pressurized tank. The SOFC may work both with green hydrogen withdrawn from the pressurized tank or with the hydrogen produced by the reform of natural gas, which is withdrawn from the gas grid.

To the best of the authors' knowledge, there are no works available in the literature presenting a dynamic analysis of an r-SOFC operating in a cogenerative mode integrated with a hospital and a PV field. For this reason, this research aims to assess whether the r-SOFC operating in a cogenerative mode and driven by green hydrogen and methane (via

steam methane reforming) is a valuable alternative to the conventional cogeneration plant based on an internal combustion reciprocating engine from an energy, environmental, and economic point of view.

2. System Layout4

Figure 1 shows the layout of the existing cogeneration plant based on a reciprocating cogeneration engine, providing thermal and electric energy to a hospital. Here, for the sake of clarity, a brief description of the existing layout is provided. Note that a detailed description of the existing layout is available in Ref. [25]. The high-temperature thermal energy provided by the CHP, i.e., the exhaust gases stream (EG), is first used to produce steam. In particular, the stream of exhaust gases (EG) is supplied to the heat exchanger HE-S-EG (Figure 1), where the steam is produced by exploiting the waste heat of EG. When the steam demand is null or the temperature of the EG leaving the heat exchanger HE-S-EG (Figure 1) is higher than $140\text{ }^{\circ}\text{C}$, the EG are delivered to the heat exchanger HE-JW-EG (Figure 1). Here, the exhaust gases stream supplies heat to the jacket water loop. When the high-temperature thermal energy, i.e., the thermal energy due to exhaust gases, provided by CHP is not sufficient to meet the hospital's steam demand, an auxiliary steam generator (SG Figure 1) is activated. The low-temperature thermal energy provided by the CHP is used to meet the building space heating, building space cooling, and sanitary hot water (SHW) thermal energy demands. In particular, the thermal energy recovered from the CHP is discharged to the heating water loop by means of the main heat exchanger (M-HE Figure 1). The hospital heating network water (Figure 1) delivers thermal energy to the heating terminals installed in each thermal zone and to the heat exchangers producing sanitary water. Note that two auxiliary boilers are considered backup systems. The thermal energy produced by CHP is also used for driving an absorption chiller (ACH). When the thermal energy available to drive ACH is not sufficient or null, an auxiliary electric-driven chiller (CH) is activated to balance the hospital building space cooling energy demand. Then, the ACH and CH cool down the chilled water network, which feeds the cooling terminal installed in the hospital, as shown in Figure 1. A cooling tower dissipates the waste heat discharged from the absorption chiller condenser and the electric chiller condenser. Note that the thermal energy is primarily used for building space heating and SHW production.

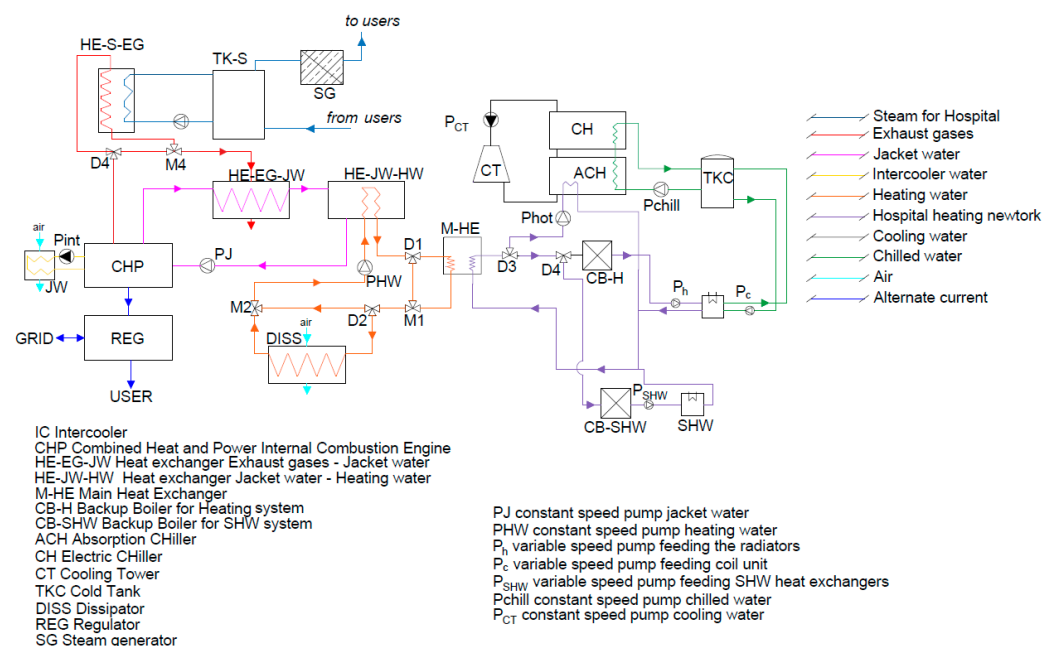


Figure 1. Existing layout based on a reciprocating engine.

Figure 2A displays the layout of a power plant based on the r-SOFC and the PV field, producing electricity, heat, and oxygen to meet the needs of the hospital. In particular, the power produced by the PV field is primarily used for balancing the hospital power load. When the PV power production is higher than the hospital power demand, the surplus electricity is used to produce renewable hydrogen (H_2). Therefore, the renewable electricity is used to drive the r-SOFC operating in an electrolyzer mode, producing hydrogen and oxygen. In particular, the cathode of the electrolyzer (Figure 2) is fed by water steam at a rated temperature of $800\text{ }^\circ\text{C}$. Note that this steam is also produced by exploiting the waste heat provided by the r-SOFC operating in the electrolyzer mode. When the cell is in operation, it produces a stream at the cathode consisting of a mixture of hydrogen (H_2) and water steam (H_2O) and a stream at the anode consisting of almost pure oxygen (O_2), as shown in Figure 2A. Given the high temperature level at the outlet of the electrodes, both the cathodic stream and anodic stream are used to produce steam by means of two heat recovery steam generators, namely HRSG-1 and HRSG-2, as shown in Figure 2A. The control strategy for managing HRSG-1 and HRSG-2 is discussed in detail in reference [46]. Note that an auxiliary steam heater (A-SH Figure 2A) is considered to achieve the setpoint temperature of the steam to be delivered to the cathode equal to $800\text{ }^\circ\text{C}$. The temperatures of the anodic and cathodic streams exiting the two heat recovery steam generators (Figure 2A) range from $90\text{ }^\circ\text{C}$ to $110\text{ }^\circ\text{C}$. Therefore, a cooling process is considered in order to reduce the compressor's electricity demand. In particular, the anodic stream is delivered to dry cooler B (Dry-B Figure 2A), which is designed to cool down the O_2 stream to a temperature close to the ambient one. The cathodic stream is delivered to the dry cooler A (Dry-A Figure 2A), where it is cooled to a temperature close to the ambient one. The cathodic stream consists of hydrogen (80%) and steam (20%). Thus, this cooling process is also able to separate the condensate water from the hydrogen stream before it is delivered to the compressor, where it is compressed up to 200 bar. At the same time, the oxygen is compressed up to 200 bar. Note that the hydrogen and oxygen compressors (C- H_2 and C- O_2 Figure 2A) are featured by four stages that are intercooled by means of the external air. When the PV power production is lower than the hospital power demand, the r-SOFC is used in the fuel cell mode to track the hospital electric load. In particular, if renewable hydrogen is available, the cell is fed by renewable hydrogen (H_2), whereas if renewable hydrogen is not available, the cell is fed by methane (CH_4) withdrawn from the gas grid. The fuel cell simultaneously produces heat and electricity. The electricity produced meets the power demand of the hospital, while the heat matches a share of the thermal load of the hospital. Note that a share of the thermal energy produced by the cell is used to preheat the flows fueling the cell. In particular, the hydrogen is delivered to the anode, while the air is delivered to the cathode, both at a temperature of $450\text{ }^\circ\text{C}$, as shown in Figure 2A. The anodic stream leaving the cell, including H_2 and H_2O , and the cathodic stream leaving the cell, including exhaust air, are mixed in the post-combustion chamber (PC Figure 2A), where catalytic combustion occurs, consuming all the unreacted hydrogen. This reaction significantly increases the temperature of the exhaust stream exiting the cell, i.e., the exhaust gas; see Figure 2A. This stream is supplied to the heat exchangers HE-EG-A and HE-EG- H_2 to preheat hydrogen and fresh air, respectively. Note that an amount of exhaust gas bypasses these heat exchangers, being directly supplied to the mixer M3. The diverter D3 is managed by means of a feedback controller. This controller manages the flow rate delivered to HE-EG-A and HE-EG- H_2 in order to obtain an outlet temperature of $450\text{ }^\circ\text{C}$ from both the heat exchangers; see Figure 2A. The exhaust air exiting from the mixer M3 is characterized by a significantly high enthalpy; therefore, this stream may be exploited to partially match the hospital thermal load. In fact, this stream is delivered to the heat exchanger HE-EG-SW (Figure 2A), where it transfers heat to the superheated water loop, i.e., water at a pressure of 10 bar; see Figure 2A.

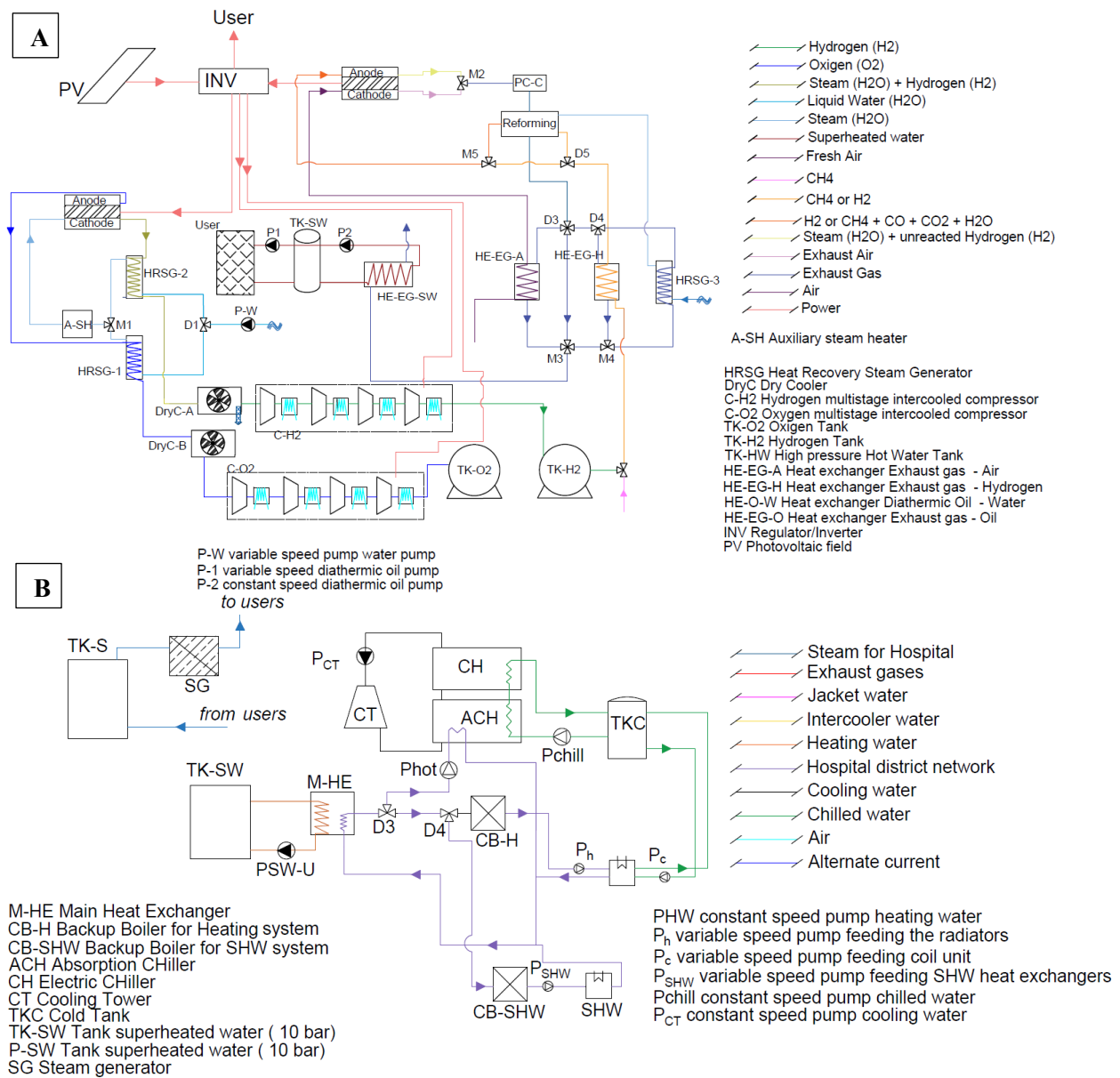


Figure 2. Proposed layout based on a reversible solid oxide fuel cell operating in cogeneration mode: (A) Reversible SOFC plant layout; (B) Layout of the hospital heating and cooling network driven by the superheated water.

When the SOFC is fed by methane (CH₄), the fuel cell operation is the same as the one described above. The only difference is the steam methane reforming that is needed to produce the hydrogen supplied to the cell. In this layout, an external steam reformer is considered. The methane is preheated by exploiting the waste heat provided by the fuel cell in an operation, reaching a temperature of 450 °C (see HE-EG-H Figure 2A). The methane is then delivered to the external steam reformer. At the same time, a suitable amount of water steam is produced in HRSG-3, exploiting the waste heat provided by the cell in operation. The temperature of the steam delivered to the external steam reformer (ESR) is equal to 450 °C. In the ESR, the methane reacts with the steam, producing H₂, CO, and CO₂. Note that a share of the thermal energy produced by the fuel cell is to drive the reaction since the steam methane reforming reaction is endothermic. In particular, the stream leaving the post combustion chamber (PC Figure 2A) first supplies thermal energy to the steam methane reformer (Figure 2A), and then it is divided by means of diverters D3 and D4 in order to feed the following heat exchangers:

- HE-GA-A, where this exhaust stream heats up the fresh air entering the plant;
- HE-EG-CH, where the exhaust stream supplies thermal energy to the methane entering the plant;
- HRSG-3, where the exhaust stream produces steam.

The diverters D3 and D4 are managed by means of a feedback controller that selects the mass flow rate to be supplied to the above-mentioned heat exchangers in order to obtain an outlet temperature of the air (H-GA-A), methane (HE-EG-CH), and steam (HRSG-3) of 450 °C. A share of the exhaust stream mass flow rate bypasses these heat exchangers and is directly delivered to the mixer M3; see Figure 2A. As mentioned before, the exhaust stream leaving the mixer M3 is characterized by high enthalpy. This thermal energy is used to partially meet the thermal energy demand of the hospital. In particular, this exhaust stream supplies heat to a superheated water loop by means of the heat exchanger HE-EG-SW; see Figure 2A. Note that the superheated water loop consists of water at 10 bar. This thermal energy is stored in the tank TK-SW. The stored thermal energy is used to match the hospital thermal energy demand for sanitary water, building space heating, and space cooling using an absorption chiller. More specifically, the superheated water (SW, Figure 2B) supplies heat to the hospital heating network by means of the main heat exchanger; see M-HE Figure 2B. The hospital heating network supplies this hot water to the heating terminals installed in each thermal zone and to the heat exchangers dedicated to sanitary water production (Figure 2B). In addition, this network also supplies hot water to an ACH, which provides cooling energy to a chilled water network (Figure 2B). Note that, as with the existing power plant layout, the plant primarily provides thermal energy to the heating terminals and the heat exchanger for sanitary water. When the remaining thermal energy is not sufficient for driving the ACH, a backup electric-driven chiller (CH, Figure 2B) is activated to balance the cooling energy demand of the hospital.

3. System Model

The existing and proposed models of the trigeneration plants serving the hospital power and thermal networks and the hospital building are developed in a TRNSYS 18 environment. This software is considered extremely reliable in modeling and simulating the real-time operation of complex power plants [15,47,48]. In fact, in TRNSYS, a wide range of technologies for diverse applications, including renewables, can be easily simulated thanks to a huge library of built-in models. The models are built in the form of energy and mass balances, allowing easy connections among them and mimicking the dynamic behavior of extremely complex systems. Moreover, TRNSYS allows one to easily integrate models that are developed by means of other software, such as MatLab 2023b. In this case, for instance, the model of the rSOFC was developed and validated in MatLab 2023b, and then it was integrated in TRNSYS to perform the simulation of the whole system. This model was then integrated in TRNSYS by means of a map of the data collected by running the simulation of the rSOFC under several different operating conditions, namely, operating current, flow rate, operating pressure, or temperature. The desired output for several possible input conditions was then used to create a map of the data, which is used as an operating map for the type. Of course, since it is a discretized map, the data regarding other operating points are obtained by interpolating the available results.

For the sake of brevity, only a brief description of the main models employed in this research is provided here. Note that the TRNSYS models of all the components are validated against the manufacturer's data and literature/experimental data. Furthermore, the models developed in MatLab by the authors are also validated using experimental data collected from the scientific literature. This circumstance also allows one to consider the validation of the model of the system as a whole [44,49–56].

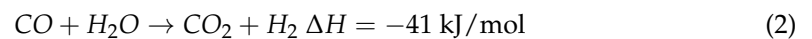
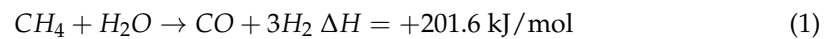
Hospital model. The model of the hospital was carefully developed and calibrated on the basis of the results of several on-site inspections. In addition, this model was validated against the measured thermal and electric energy consumptions of the hospital. The geometrical model of the hospital was developed using the software Google SketchUp

TRNSYS3d plug-in. Then, the geometrical model of the hospital was imported into TRNSYS18 by means of Type 56 in order to dynamically simulate the energy performance of the hospital. Type 56 allows one to carefully model the thermophysical features of the studied building. In particular, Type 56 performs the building energy balances considering the building orientation, the internal gains, the solar gains, and the features of the envelope. Note that this type has proven to be extremely reliable and accurate in modeling the building's energy performance; see Refs [15,57–60]. A detailed discussion about the hospital model calibration is provided in Ref. [25].

Reciprocating combined heat and power engine. The reciprocating engine is modeled by means of Type 907, which carefully mimics the real-time operation of an internal combustion engine; see Ref. [15]. Note that the real-time operations of the existing CHP layout are calibrated against the measured data regarding the energy performance of the internal combustion engine and the heating and cooling networks.

Reversible solid oxide fuel cell. The model of the r-SOFC was not available in the TRNSYS library; thus, the r-SOFC model was developed in-house. A detailed description of this model is provided in Ref. [19].

Steam methane reforming (SMR). The SMR model was developed in-house. The reaction is featured by two stages: the decomposition of methane into hydrogen and carbon monoxide and the shift reaction [61–63].



The degree of demethanation is given by the following equation [63]:

$$V_{CH_4} = \frac{n_{CH_4,in} - n_{CH_4,out}}{n_{CH_4,in}} \quad (3)$$

where $n_{CH_4,in}$ and $n_{CH_4,out}$ are the inlet molar flow rate and outlet molar flow rate, respectively.

Therefore, the degrees of reaction of the first phase of reforming, x , and the degree of reaction of the shift reaction, y , are assessed according to the following equations [63]:

$$x = V_{CH_4} \cdot n_{CH_4,in} \quad (4)$$

$$K_{shift}(T) = \frac{(n_{CO_2,i} + y) \cdot (n_{H_2,i} + 3x + y)}{(n_{H_2O,i} - x - y) \cdot (n_{CO,in} + x - y)} \quad (5)$$

where K_{shift} is the equilibrium constant of the shift reaction. Ref. [61] provides a detailed description of such model.

Thermoeconomic Model

The primary energies of both the existing and the proposed plant are evaluated as follows:

$$\begin{aligned} PE_{RS} &= \sum_t \left[\left(E_{el,fromGRID} - E_{el,toGRID} \right) \frac{1}{\eta_{el}} + \left(\frac{E_{th,CB-H} + E_{th,CB-DHW}}{\eta_B} + \frac{E_{th,SG}}{\eta_{SG}} \right) + V_{NG,CHP} LHV_{NG} \right]_t \\ PE_{PS} &= \sum_t \left[\left(E_{el,fromGRID} - E_{el,toGRID} \right) \frac{1}{\eta_{el}} + \left(\frac{E_{th,CB-H} + E_{th,CB-DHW}}{\eta_B} + \frac{E_{th,SG}}{\eta_{SG}} \right) + V_{NG,SOFC} LHV_{NG} \right]_t \\ PES &= \frac{PE_{RS} - PE_{PS}}{PE_{RS}} \\ R_{renew} &= 100 - \frac{\sum_t \left[\frac{E_{el,fromGRID}}{\eta_{el}} + \left(\frac{E_{th,CB-H} + E_{th,CB-DHW}}{\eta_B} + \frac{E_{th,SG}}{\eta_{SG}} \right) + V_{NG,SOFC} LHV_{NG} \right]_t}{PE_{RS}} \end{aligned} \quad (6)$$

where $V_{NG,CHP}$ represents the natural gas delivered to the CHP, whereas $V_{NG,SOFC}$ represents the natural gas delivered to the SOFC when no renewable hydrogen is available. $E_{el,fromGRID}$ and $E_{el,toGRID}$ represent the electricity withdrawn and delivered to the grid.

The operative costs of RS and PS are evaluated according to the following equations:

$$C_{RS} = \sum_t \left[j_{el,fromGRID} E_{el,fromGRID} + j_{NG} \left(\frac{E_{th,CB-H} + E_{th,CB-DHW}}{LHV_{NG}\eta_B} + \frac{E_{th,SG}}{LHV_{NG}\eta_{SG}} + V_{NG,CHP} \right) + m \right]_t \quad (7)$$

$$C_{PS} = \sum_t \left[j_{el,fromGRID} E_{el,fromGRID} - j_{el,toGRID} E_{el,toGRID} + j_{NG} \left(\frac{E_{th,CB-H} + E_{th,CB-DHW}}{LHV_{NG}\eta_B} + \frac{E_{th,SG}}{LHV_{NG}\eta_{SG}} + V_{NG,SOFC} \right) + m - j_{O_2} M_{O_2} \right]_t$$

Note that the oxygen produced by the cell operating in the electrolyzer mode is assumed to be exported at a specific price of (j_{O_2}) 2 EUR/kg, [64–67]. The simple payback period is evaluated carefully to assess the capital cost of all of the technologies needed to replace the reciprocating engine with the r-SOFC.

$$C_{tot} = I_{PV} + I_{SOFC} + I_{TK-H_2} + I_{C1} + I_{C2} + I_{HEs} + I_{HRSG} + I_{SG} + I_{TK-SW} + I_{pumps} + I_{dryCs} + I_{A-SH} \quad (8)$$

The main terms of this equation are summarized in Table 1.

Table 1. Design and operating parameters.

Parameter	Description	Value	Unit
$j_{el,fromGRID}$	Electricity purchasing cost	0.23	EUR/kWh
$j_{el,toGRID}$	Electricity energy exporting cost	0.06	EUR/kWh
j_{NG}	Natural gas purchasing price	1.30	EUR/Sm ³
j_{O_2}	Oxygen purchasing price	2.00 [64–67]	EUR/kg
LHV_{H_2}	Hydrogen lower heating value	3.00	kWh/Sm ³
LHV_{CH_4}	Natural gas lower heating value	120.00	MJ/kg
LHV_{CH_4}	Natural gas lower heating value	9.59	kWh/Sm ³
J_{PV}	PV cost	1000 [15]	EUR/kW
J_{REF}	External steam methane reformer capital cost	259.0 [68]	M EUR/MW _{NG}
J_{SOFC}	r-SOFC cost	3000 [69]	EUR/kW
J_{TK-H_2}	Hydrogen tank cost	500 [70]	EUR/kg
I_c	Compressor capital cost	$C_C = 5840 \cdot (P_{el,C,rated})^{0.82}$ [71]	EUR/compr
I_{HE}	Heat exchanger capital cost	$C_{HE} = 130 \cdot 1.4 \cdot [(A_{HE}/0.093)^{0.78}]$ [72]	EUR/HE
I_{TK-SW}	Superheated water capital cost	$C_{TK} = 494.9 + 0.808 \cdot V_{TK-O}$ [73]	EUR
J_{HRSG}	Heat recovery steam generator	0.368 [74,75]	M EUR/HRSG
J_{dryC}	Dry cooler specific cost	200 [76]	EUR/kW
J_{A-SH}	Auxiliary steam heater specific cost	125 [77]	EUR/kW
η_{el}	Conventional thermo-electric power plant efficiency	46	%
η_B	Boiler efficiency	75	%
η_{SG}	Steam generator efficiency	98	%
η_{A-SH}	Steam heater efficiency	98	%
η_{inv}	District inverter efficiency	95	%

4. Case Study

The selected hospital is located near the city of Bari, in southern Italy. This hospital hosts almost 603 beds, and it is one of the largest hospitals in the south of Italy. For the sake of brevity, only the main features of the existing and proposed plants are provided. Table 2 lists the main technical data for the technologies discussed in this section, both for the existing and proposed systems. The features of the hospital building are available in Ref. [25]. The current power plant of the hospital is based on a CHP, which follows the hospital power load. This CHP simultaneously provides thermal energy and electric energy. The thermal energy is used to meet the thermal energy demand of the hospital to build space heating, produce sanitary water production, and produce steam. In addition, this

thermal energy is also used to drive an ACH. Note that the thermal energy recovered from the CHP is primarily used for heating purposes. Therefore, ACH is only activated when the heating energy demand of the hospital is null or there is a sufficient thermal energy surplus to drive the ACH. Three electric chillers are installed as a backup system. Table 3 shows the yearly electricity and thermal energy consumption of the hospital.

Table 2. Main component data and features.

Component	Parameter	Description	Value	Unit
CB _H	$P_{th,CBH}$	Rated capacity of CB _H	6.20	MW _{th}
	$T_{set,CB}$	Set point temperature for CB _H	80	°C
	η_{CBDHW}	CB _H efficiency	86	%
CB _{SHW}	$P_{th,CBSHW}$	Rated CB for SHW thermal flow rate	0.70	MW _{th}
	$T_{set,CBSHW}$	Set point temperature for CB _{SHW}	80	°C
	η_{CBDHW}	CB _{SHW} efficiency	0.86	%
SG	$P_{th,SG}$	Rated capacity steam generator	6880	
	η_{SG}	SG efficiency	90	%
Cogenerator [78]	-	Model Name	JMS-612-GS-N.L.	
	-	Manufacturer	GE Jenbacher GmbH & Co OHG (Austria)	
	$P_{th,CHP}$	Rated thermal capacity	1.90	
	$P_{el,CHP}$	Rated electrical capacity	2.00	MW
	$P_{th,input}$	Rated fuel input	4.42	
	η_{el}	Rated electrical efficiency	45.2	
	η_{th}	Rated thermal efficiency	43.0	%
	η	Global rated efficiency	88.3	
ACH	P_{rated}	Rated cooling capacity	0.77	MW _{th}
	COP	Rated coefficient of performance	0.75	-
CH	$P_{th,CH}$	Rated cooling capacity	9.00	MW _{th}
	COP	Rated coefficient of performance	5.95	-
CT	$P_{th,CT}$	Rated thermal capacity of CT	1.79	MW _{th}
	$N_{f,CT}$	Number of fans of CT	2	-
	$P_{el,fan,CT}$	Fan power of CT	15	kW
PV	η_{PV}	Module efficiency	0.20	-
	$P_{rated,PV}$	PV panel rated power	6.00	MW
	A_{tot}	PV field area	30,000	m ²
r-SOFC	$Press_{cell}$	Cell operative pressure	1	
	$N_{SOFC,cell}$	Number of cells in series	8	
	$N_{SOFC,par}$	Number of stacks in parallel	4166	
Reformer	$P_{el,SOFC}$	Rated fuel cell/electrolyzer capacity	2.00	MW
	$Press_{Ref}$	Reformer operative pressure	1	bar
	T_{rated}	Rated fuel feeding temperature	450	°C
Tank TK-H2	Φ	Rated enthalpy flow of fuel	3.63	MW
	V_{TK-H2}	Tank Volume	28	m ³
	$Press_{TK-H2}$	Max tank pressure	200	bar

Table 2. Cont.

Component	Parameter	Description	Value	Unit
Compressor C-H2	$\eta_{compressor}$	Compressor isentropic efficiency	80	%
	N_{stages}	Number of stages	4	-
	β	Compression ratio	3.75	-
	$Press$	Rated pressure	200	bar
Compressor C-O2	$\eta_{compressor}$	Compressor isentropic efficiency	80	%
	N_{stages}	Number of stages	4	-
	β	Compression ratio	3.65	-
	$Press$	Rated pressure	150	bar

Table 3. Existing hospital power plant energy consumption, operating costs, and emissions.

Parameter	Value	Unit
$E_{th,heat}$	7.33	GWh _{th} /y
$E_{th,SG}$	8.61	GWh _{th} /y
$E_{th,SHW}$	0.47	GWh _{th} /y
$E_{th,cool}$	9.71	GWh _{th} /y
$E_{el,LOAD}$	16.36	GWh _{el} /y
PE	46.41	GWh/y
C	6.21	M EUR/y
CO_2	8388	tCO ₂ /y

In the system proposed, the reciprocating engine is replaced with an r-SOFC integrated with an external steam reformer and a PV field. Then, the renewable power provided by the PV field is used to meet the hospital's power demand. During this phase, the thermal load of the hospital is met by means of the auxiliary boilers (CB-H and CB-SHW) and three electric chillers. The surplus electricity is used to produce renewable hydrogen, which is stored in a tank in gaseous form. When the PV power production is null or low, the renewable hydrogen produced and stored is used to drive the fuel cell. The thermal energy provided by the fuel cell is used to meet the hospital's thermal energy demand. The thermal energy recovered is exploited to drive the ACH, which is the same as that for the existing layout. The thermal energy recovered is primarily used for heating purposes. When renewable hydrogen is not available, the methane is withdrawn from the gas grid and delivered to a steam methane reformer to produce hydrogen that will be supplied to the fuel cell.

5. Results

The proposed power plant based on r-SOFC integrated with a PV and methane steam reformer achieves very promising performance, resulting in an interesting solution for replacing the conventional CHP. In fact, the proposed power plant is able to significantly reduce the primary energy consumption of the hospital, achieving a PES of 30%; see Table 4. In particular, 97% of the hospital electric load ($E_{el,load}$) is met by the electricity produced by the proposed power plant, i.e., $E_{el,self}$ is equal to 16.60 GWh/y; see Table 4. However, the renewable share of energy accounts for 50% of $E_{el,self}$. These results are clearly explained in Figure 3. In fact, according to the SOFC operating strategy, i.e., the electric load tracking, the r-SOFC matches the hospital power load ($P_{el,load}$) for the majority of the day. During the central part of the day, when the PV field achieves the peak of electricity production ($P_{el,PV}$), i.e., 5000 kW, $P_{el,load}$ is directly balanced by the renewable power. At the same time, the surplus electricity is delivered to the electrolyzer, which produces renewable

hydrogen (see $P_{el,toSOEC}$ Figure 3). Note that the electricity delivered to SOFC operating in the electrolyzer mode is constantly equal to 2000 kW, which is the rated capacity of the cell. The renewable hydrogen ($P_{e,fromSOFC(H2)}$) is exploited during the evening when the PV production decreases to zero. In particular, SOFC fed by renewable hydrogen is able to meet the hospital load for almost 4 h from 16:00 to 20:00. In conclusion, the hospital is driven by renewable electricity for roughly 13 h, i.e., 54% of the day. The surplus electricity delivered to the grid ($P_{el,toGRID}$) is almost limited, accounting for 0.50 GWh/y, i.e., less than 7% of PV electricity production. In fact, according to the trends displayed in Figure 3, the system is able to handle the majority of PV electricity production (Table 4).

Table 4. Yearly results.

Parameter	Unit	RS	PS
PE_{CHP}	GWh/year	35.62	17.46
$E_{el,load}$	GWh/year	16.89	18.26
$E_{el,CHP}$	GWh/year	15.03	-
$E_{el,PV}$	GWh/year	-	10.20
$E_{el,SOEC}$	GWh/year	-	2.08
$E_{el,SOFC(H2)}$	GWh/year	-	0.98
$E_{el,SOFC(CH4)}$	GWh/year	-	8.58
$E_{el,fromGRID}$	GWh/year	1.85	1.06
$E_{el,toGRID}$	GWh/year	0.00	0.48
$E_{el,self}$	GWh/year	15.03	17.19
$E_{th,B}$	GWh/year	2.60	3.77
$E_{th,SG}$	GWh/year	3.39	8.61
$E_{th,CHP2Steam}$	GWh/year	5.22	0.00
$E_{th,CHP2M-HE}$	GWh/year	7.30	5.01
$E_{th,SOFC(H2)2M-HE}$	GWh/year	-	4.29
$E_{th,SOFC(CH4)2M-HE}$	GWh/year	-	0.72
$E_{th,M-HE2ACH}$	GWh/year	2.96	1.05
$E_{th,ACH}$	GWh/year	2.10	0.78
$E_{th,CH}$	GWh/year	9.48	10.49
$E_{el,CH}$	GWh/year	1.57	1.71
PE_{tot}	GWh/year	46.41	30.74
ΔPE	GWh/year	-	15.67
PES	%	-	29.64
R_{renew}	%	-	27.33
$V_{NG,CHP}$	Sm ³ /year	3.71×10^6	
$V_{NG,SOFC}$	Sm ³ /year		1.82×10^6
$V_{NG,aux}$	Sm ³ /year	0.71×10^6	1.45×10^6
V_{NG}	Sm ³ /year	4.42×10^6	3.27×10^6
ΔMx	t/year	-	2561.57
ΔMx	%	-	30.53
ΔC	M EUR/year	-	2.72
C	M EUR	-	12.84
SPB	years	-	4.71
PI		-	0.69
NPV	M EUR/year	-	8.71

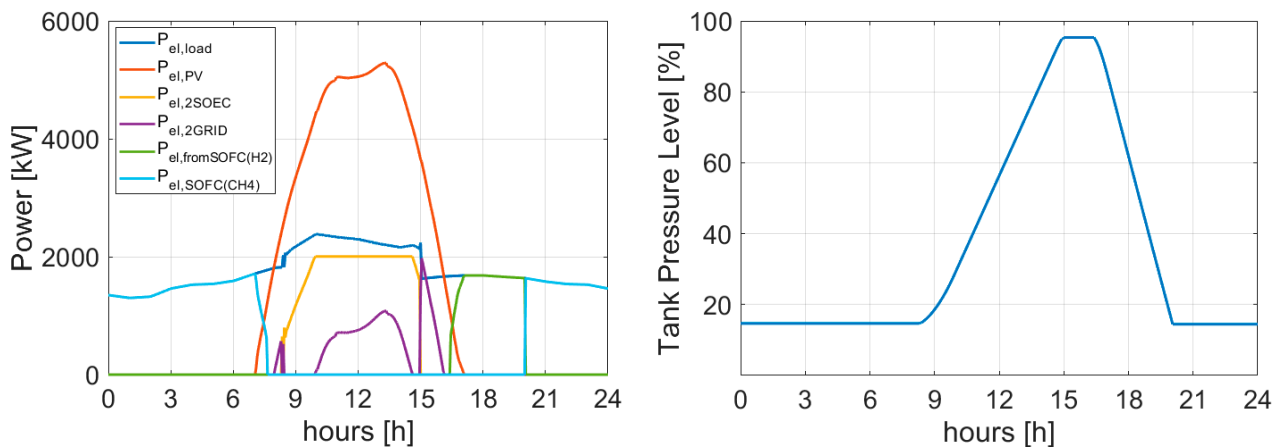


Figure 3. Dynamic results: power flows and pressure level of the hydrogen tank.

Concerning the thermal energy performance of the proposed plant, considering that the PV power production directly matches the hospital power load during the central part of the day, the activation of the auxiliary boilers and steam generator compared with the reference system increases; see Figure 4. Moreover, when the SOFC is driven using the methane withdrawn from the grid, a share of the thermal energy produced by the cell is used to run the steam methane reformer (SMR) and produce the steam to be delivered to the SMR in order to produce hydrogen from methane. Then, the available thermal energy is lower compared with the one provided by the SOFC, which is directly fueled by hydrogen or conventional CHP. In fact, when steam methane reform is in operation, the thermal efficiency is lower. For example, from 16:00 to 17:00, when SOFC exploits the green hydrogen, η_{th} is roughly equal to 38%, whereas from 17:00, when the SOFC is supplied by the hydrogen produced by means of SMR, η_{th} is equal to 26%; see Figure 4. For these reasons, the thermal energy supplied by the hospital boiler $E_{th,B}$ passes from 2.60 GWh/y (RS) to 3.96 GWh/y (PS). Figure 5 confirms these trends on a monthly basis. It is worth noting that the electrical efficiency of the SOFC is lower when the cell uses hydrogen, i.e., $\eta_{el,SOFC(H_2)} = 48\%$ vs. $\eta_{el,SOFC(CH_4)} = 51\%$ (Table 4). This result is due to the fact that the cell fed by methane operates for a longer time at a partial load. In fact, the cell's electric efficiency increases as the cell load decreases. In particular, the cell fed by methane mainly operates during the evening and night, when the PV power production is null and the green hydrogen is not available. During these hours, the electric load of the hospital is lower compared to the central part of the day when hospital activities are at capacity. In conclusion, Figure 5 confirms the advantages of the proposed plant with respect to the conventional power plant. In fact, the thermal energy demand of the hospital is at a minimum during the summer season, when solar production is at its maximum. During the central part of a typical day, the PV power production directly matches the hospital power load, and the surplus electricity is supplied to SOFC operating in an electrolyzer mode, while the thermal load of the hospital is met by the auxiliary system burning fossil methane. However, during the summer season, when PV production is greater, the increase in thermal energy provided by the auxiliary system is limited because of the limited demand for heating energy. In fact, according to Figure 5, the thermal energy provided by the SOFC fed by methane matches the larger part of the user's thermal energy demand, i.e., more than 60% from May to September. Moreover, during this period, the share of thermal energy matched by the auxiliary boilers is minimal, i.e., lower than 8%. At the same time, renewable electricity matches more than 70% of the hospital demand from May to September. In addition, during these months, the cooling demand of the hospital is mainly matched by the electric chiller driven by the renewable electricity produced by the PV field.

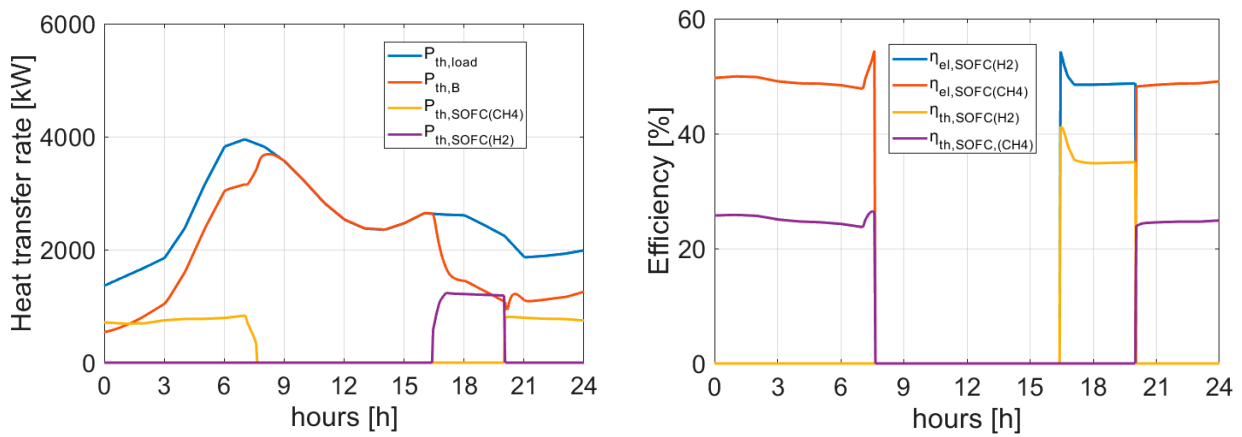


Figure 4. Dynamic results: heat transfer rates and efficiency of the fuel cell.

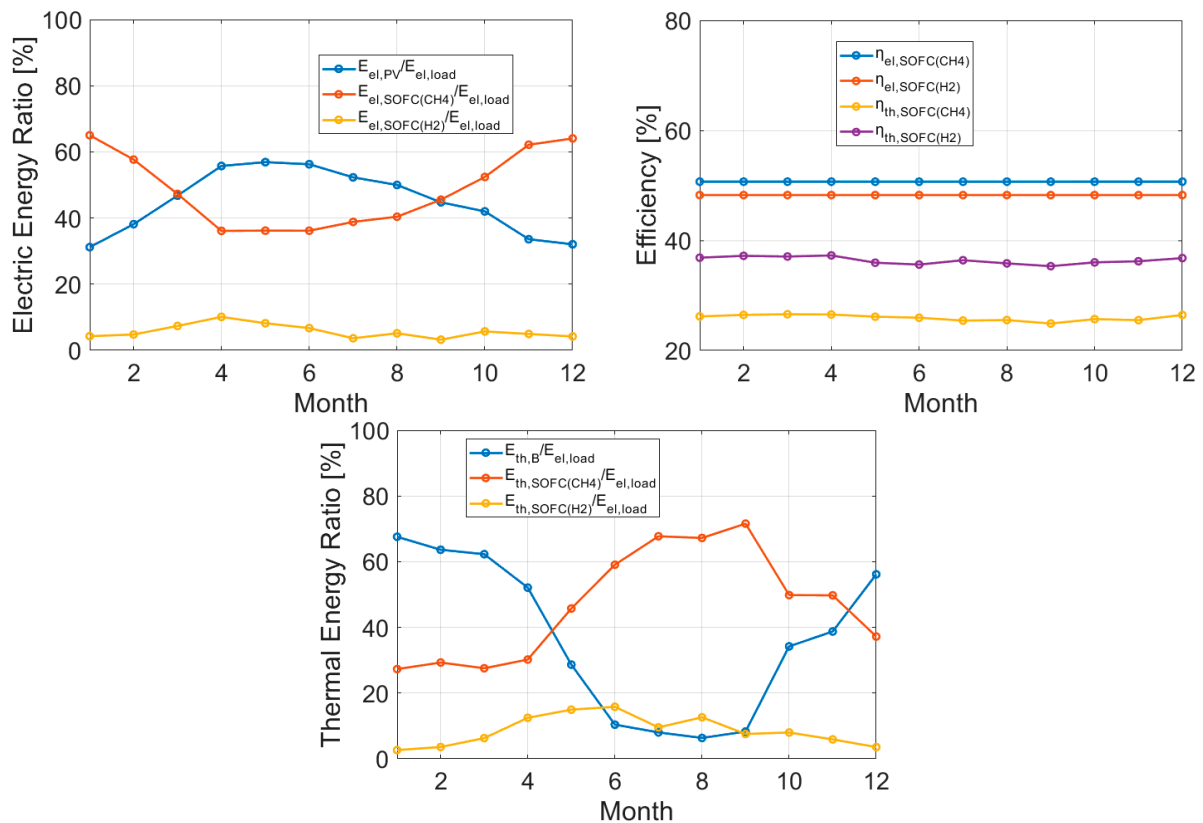


Figure 5. Monthly results: main electric and thermal energy ratios and efficiency of the fuel cell.

From an economic point of view, as discussed before, the proposed power plant is able to dramatically reduce the amount of electricity withdrawn from the grid. Despite the fact that the proposed plant is featured by a greater amount of thermal energy supplied by the auxiliary systems (boilers and steam generator), compared with the RS, the natural gas consumption of the proposed plant significantly decreases. This trend is due to the reasons discussed above in detail. In fact, the natural gas demand for the auxiliary systems exhibits a limited increase, passing from $0.71 \times 10^6 \text{ Sm}^3/\text{y}$ to $1.49 \times 10^6 \text{ Sm}^3/\text{y}$, whereas the natural gas demand of CHP decreases by 54%, passing from $3.71 \times 10^6 \text{ Sm}^3/\text{y}$ ($V_{NG,CHP}$) to $1.70 \times 10^6 \text{ Sm}^3/\text{y}$ ($V_{NG,SOFC}$). Thus, the electric energy produced by the PV field and used to produce hydrogen and directly match the hospital load is crucial to reducing the consumption of natural gas. For these reasons, given the high natural gas purchasing cost, i.e., j_{NG} 1.30 EUR/ Sm^3 , the proposed layout leads to significant economic savings.

In addition, the oxygen produced by the r-SOFC operating in the electrolyzer mode is exported at a specific price of 2.00 EUR/kg (Table 1 [46]). Then, despite the high capital costs, an interesting payback period of 6.13 years was obtained. Even not considering the savings due to the oxygen export, the SPB is still interesting, being equal to 9.50 years. The gains due to oxygen export account for 35% of the system's savings.

Sensitivity Analysis

In order to assess the capacity of r-SOFC and how the PV affects the overall performance of the proposed system, a sensitivity analysis is carried out. In particular, the capacity of the PV field is changed from 1.50 MW to 18.00 MW, while the capacity of the r-SOFC is varied from 0.50 MW to 6.00 MW.

Figure 6 displays the results of the PV field capacity as varied. As expected, the increase in the PV capacity leads to an improvement in the energy performance of the whole plant; the PES grows as the PV capacity increases. In fact, when the PV capacity is equal to 12.00 MW, the PES achieves a value of 71%; see Figure 6. The minimum SPB is achieved for a PV capacity of 9.00 MW. After this value, as the PV capacity increases, the SPB slightly decreases. This result is due to the fact that when the PV capacity increases from 1.50 MW to 9.00 MW, the self-consumed electricity ($E_{el,Self}$) significantly increases, passing from 87% to 97%. A further increase in the PV capacity leads to a negligible increase in the self-consumed energy. This means that a PV of 9.00 MW is able to meet almost all of the electricity demands of the selected user. Then, as the PV capacity increases from 9.00 MW, the increases in the capital cost due to the larger PV field are not balanced by the consequential benefits due to the further renewable production.

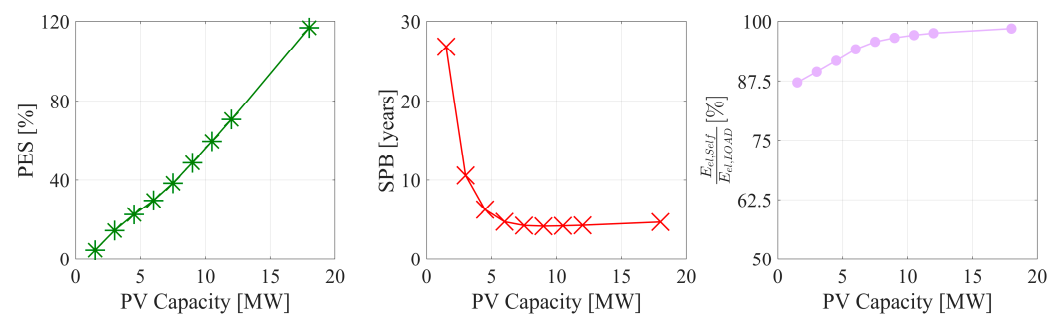


Figure 6. Sensitivity analysis: variation of the photovoltaic field capacity.

Figure 7 displays the results achieved by varying the capacity of the reversible fuel cell. As the cell capacity varies, the R_{renew} index increases, reaching the maximum value of 27.60% for an r-SOFC capacity of 2.50 MW. Note that when the capacity of the reversible fuel cell approaches 2.00 MW, the R_{renew} index is quite stable at around 27.50%; see Figure 7. These results rely on the fact that the increase in cell capacity allows the system to maximize the use of the PV renewable electricity, producing green hydrogen. However, as shown in Figure 3, when the capacity of the cell is equal to 2.00 MW, the surplus renewable electricity not used and delivered to the grid is limited. Therefore, a further increase in the cell capacity from 2.50 MW does not lead to a significant increase in renewable hydrogen production. For these reasons, from 2.00 MW to 3.50 MW, the R_{renew} index is quite stable; see Figure 7. However, as the cell capacity rises beyond 4.00 MW, the R_{renew} index dramatically worsens. This result relies on the minimum activation power needed to drive the cell; this power is assumed to be equal to 30% of the cell's rated capacity [46,76,79–81]. Therefore, when the capacity of the cell is 6.00 MW, the electricity delivered to the cell is reduced. This trend is also clearly explained in Figure 7. In fact, when the capacity rises beyond 4.00 MW, the share of the load met by the self-produced electricity ($E_{el,self}$) dramatically falls; see Figure 7.

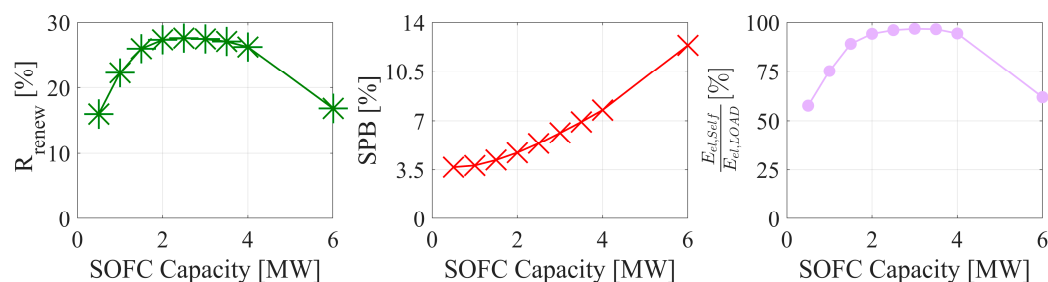


Figure 7. Sensitivity analysis: variation of the reversible solid oxide fuel cell capacity.

From an economic point of view, the cell has a dramatically high capital cost. As the cell capacity rises, the investment costs skyrocket. For this reason, the economic performance worsens, i.e., the SPB worsens.

6. Conclusions

This paper assesses the energy, environmental, and economic performance of a novel cogeneration layout based on a reversible solid oxide fuel cell and a photovoltaic field serving a huge hospital. In particular, the existing hospital plant is based on an internal combustion engine of 2.00 MW that burns natural gas and produces electricity and thermal energy. The proposed system considers the replacement of the internal combustion engine with a 2.00 MW reversible solid oxide fuel cell. In particular, the electric load of the hospital is met by exploiting the renewable electricity provided by the photovoltaic field of 6.00 MW. The surplus power is used to produce hydrogen. Thus, when photovoltaic power production is scarce or unavailable, the renewable hydrogen is delivered to the fuel cell to meet the hospital's electric load. At the same time, the thermal energy recovered by the fuel cell is used to meet the hospital's thermal energy demand. However, when renewable hydrogen is not available, the fuel cell is fed by methane via methane steam reforming. The simulation model is developed in TRNSYS 18 and calibrated and validated against the measured data.

The main results achieved in the paper are summarized below.

- The proposed layout is extremely promising, as it was able to reduce the natural gas consumption of the hospital by almost 30%.
- The proposed system achieves a primary energy savings of 32%.
- From an economic point of view, despite the remarkable capital cost of EUR 17.7 M, the proposed plant achieves an interesting simple payback of 6.5 years.
- The PV field capacity should be equal to 9.00 MW to maximize the economic performance of the proposed plant.

Author Contributions: F.C.: Conceptualization, Formal analysis, Funding acquisition, Methodology, Project administration, Resource, Software, Supervision, Writing—review and editing. F.L.C.: Conceptualization, Data curation, Formal analysis, Funding acquisition, Investigation, Methodology, Project administration, Resource, Software, Supervision, Validation, Visualization, Writing—original draft, Writing—review and editing. L.C.: Data curation, Investigation, Software, Visualization, Writing—original draft, Writing—review and editing. M.D.d.: Data curation, Investigation, Resource, Supervision, Validation, Visualization, Writing—review and editing. M.V.: Data curation, Investigation, Methodology, Resource, Validation, Writing—review and editing. All authors have read and agreed to the published version of the manuscript.

Funding: This received no external funding.

Data Availability Statement: The data used for this research can be shared if requested.

Acknowledgments: The authors gratefully acknowledge the partial financial support of the project “Sustainable Energy Networks” CUP E65F21003190003. PRIN 2020: OPTIMISM—Optimal refurbishment design and management of small energy micro-grids, funded by the Italian Ministry of University and Research (MUR).

Conflicts of Interest: The authors declare no conflict of interest.

Nomenclature

AEC	Alkaline electrolyzer cell
AFC	Alkaline fuel cell
A-SH	Auxiliary steam heater
ASR	Area specific resistance (w/cm^2)
C	Cost (EUR)
CHP	Cogeneration of heat and power
CCHPO	Combined cooling, heating, power, and oxygen system
E	Energy (kWh) or (MWh)
F	Faraday's constant (C/mol)
GHG	Greenhouse gases
HE	Heat exchanger
HSS	Hydrogen storage system
i	Current density (mA/cm^2)
LCOE	Levelized cost of energy (EUR)
n	Molar flow rate (mol/s)
NPV	Net present value (kEUR)
OLR	Organic loading rate ($kgCOD/(L d)$)
p	Pressure (bar)
P	Power (kW)
PE	Primary energy (MWh)
PEM	Proton exchange membrane
PES	Primary energy saving (%)
PI	Profit index (%)
PV	Photovoltaic
R	Gas constant ($J/mol K$)
RES	Renewable energy system
rSOFC	Reversible solid oxide fuel cell
SMR	Steam methane reforming
SOEC	Solid oxide electrolyzer cell
SOFC	Solid oxide fuel cell
SPB	Simple pay back (years)
T	Temperature ($^{\circ}C$) or (K)
V	Volume (m^3)
Subscripts	
aux	Auxiliary
EE	Electric energy
fromGRID	Referred to electricity withdrawn from the electric grid
NG	Natural gas
toGRID	Referred to electricity exported to the electric grid
Greek symbols	
β	Compression factor
η	Efficiency (adim.)

References

- Zhang, S.-C.; Yang, X.-Y.; Xu, W.; Fu, Y.-J. Contribution of nearly-zero energy buildings standards enforcement to achieve carbon neutral in urban area by 2060. *Adv. Clim. Change Res.* **2021**, *12*, 734–743. [[CrossRef](#)]
- Gaspard, A.; Chateau, L.; Laruelle, C.; Lafitte, B.; Léonardon, P.; Minier, Q.; Motamedi, K.; Ougier, L.; Pineau, A.; Thiriot, S. Introducing sufficiency in the building sector in net-zero scenarios for France. *Energy Build.* **2023**, *278*, 112590. [[CrossRef](#)]
- Wang, T.; Li, X.; Liao, P.-C.; Fang, D. Building energy efficiency for public hospitals and healthcare facilities in China: Barriers and drivers. *Energy* **2016**, *103*, 588–597. [[CrossRef](#)]
- CADDET; IEA; OECD. *Saving Energy with Energy Efficiency in Hospitals*; CADDET: Sittard, The Netherlands, 2005.
- García-Sanz-Calcedo, J.; Al-Kassir, A.; Yusaf, T. Economic and Environmental Impact of Energy Saving in Healthcare Buildings. *Appl. Sci.* **2018**, *8*, 440. [[CrossRef](#)]

6. Mohd Daud, A.K.; Ahmad, E.Z.; Razak, T.R.; Jarimi, H. Expertise-based systematic guidelines for chiller retrofitting in healthcare facilities. *J. Build. Eng.* **2023**, *74*, 106708. [CrossRef]
7. Shen, C.; Zhao, K.; Ge, J.; Zhou, Q. Analysis of Building Energy Consumption in a Hospital in the Hot Summer and Cold Winter Area. *Energy Procedia* **2019**, *158*, 3735–3740. [CrossRef]
8. Chung, M.; Park, H.-C. Comparison of building energy demand for hotels, hospitals, and offices in Korea. *Energy* **2015**, *92*, 383–393. [CrossRef]
9. Atienza-Márquez, A.; Domínguez Muñoz, F.; Fernández Hernández, F.; Cejudo López, J.M. Domestic hot water production system in a hospital: Energy audit and evaluation of measures to boost the solar contribution. *Energy* **2022**, *261*, 125275. [CrossRef]
10. Balali, A.; Valipour, A. Prioritization of passive measures for energy optimization designing of sustainable hospitals and health centres. *J. Build. Eng.* **2021**, *35*, 101992. [CrossRef]
11. Short, C.A.; Lomas, K.J.; Giridharan, R.; Fair, A.J. Building resilience to overheating into 1960's UK hospital buildings within the constraint of the national carbon reduction target: Adaptive strategies. *Build. Environ.* **2012**, *55*, 73–95. [CrossRef]
12. Kim, S.H.; Augenbroe, G. Decision support for choosing ventilation operation strategy in hospital isolation rooms: A multi-criterion assessment under uncertainty. *Build. Environ.* **2013**, *60*, 305–318. [CrossRef]
13. As, M.; Bilir, T. Enhancing energy efficiency and cost-effectiveness while reducing CO₂ emissions in a hospital building. *J. Build. Eng.* **2023**, *78*, 107792. [CrossRef]
14. Koirala, B.; Hers, S.; Morales-España, G.; Özdemir, Ö.; Sijm, J.; Weeda, M. Integrated electricity, hydrogen and methane system modelling framework: Application to the Dutch Infrastructure Outlook 2050. *Appl. Energy* **2021**, *289*, 116713. [CrossRef]
15. Cappiello, F.L.; Erhart, T.G. Modular cogeneration for hospitals: A novel control strategy and optimal design. *Energy Convers. Manag.* **2021**, *237*, 114131. [CrossRef]
16. Biglia, A.; Caredda, F.V.; Fabrizio, E.; Filippi, M.; Mandas, N. Technical-economic feasibility of CHP systems in large hospitals through the Energy Hub method: The case of Cagliari AOB. *Energy Build.* **2017**, *147*, 101–112. [CrossRef]
17. Isa, N.M.; Tan, C.W.; Yatim, A. A comprehensive review of cogeneration system in a microgrid: A perspective from architecture and operating system. *Renew. Sustain. Energy Rev.* **2018**, *81*, 2236–2263. [CrossRef]
18. Evins, R.; Orehounig, K.; Dorer, V.; Carmeliet, J. New formulations of the 'energy hub' model to address operational constraints. *Energy* **2014**, *73*, 387–398. [CrossRef]
19. Calise, F.; Cappiello, F.L.; Cimmino, L.; Dentice d'Accadia, M.; Vicidomini, M. Dynamic Simulation and Thermo-economic Analysis of a Hybrid Renewable System Based on PV and Fuel Cell Coupled with Hydrogen Storage. *Energies* **2021**, *14*, 7657. [CrossRef]
20. Renedo, C.J.; Ortiz, A.; Mañana, M.; Silió, D.; Pérez, S. Study of different cogeneration alternatives for a Spanish hospital center. *Energy Build.* **2006**, *38*, 484–490. [CrossRef]
21. Alexis, G.; Liakos, P. A case study of a cogeneration system for a hospital in Greece. Economic and environmental impacts. *Appl. Therm. Eng.* **2013**, *54*, 488–496. [CrossRef]
22. Gimelli, A.; Muccillo, M. Optimization criteria for cogeneration systems: Multi-objective approach and application in an hospital facility. *Appl. Energy* **2013**, *104*, 910–923. [CrossRef]
23. Ghoreishinejad, M.; Deymi-Dashtebayaz, M.; Norani, M. Proposal and multi-objective optimization of a CCHP system based on heat recovery from oxygen generator in hospitals: A case study. *J. Clean. Prod.* **2023**, *421*, 138549. [CrossRef]
24. Chen, X.; Chen, Y.; Zhang, M.; Jiang, S.; Gou, H.; Pang, Z.; Shen, B. Hospital-oriented quad-generation (HOQG)—A combined cooling, heating, power and gas (CCHPG) system. *Appl. Energy* **2021**, *300*, 117382. [CrossRef]
25. Calise, F.; Cappiello, F.L.; Dentice d'Accadia, M.; Libertini, L.; Vicidomini, M. Dynamic simulation and thermo-economic analysis of a trigeneration system in a hospital application. *Energies* **2020**, *13*, 3558. [CrossRef]
26. Izzeldin, M.; Muradoğlu, Y.G.; Pappas, V.; Petropoulou, A.; Sivaprasad, S. The impact of the Russian-Ukrainian war on global financial markets. *Int. Rev. Financ. Anal.* **2023**, *87*, 102598. [CrossRef]
27. Lo, G.-D.; Marcelin, I.; Bassène, T.; Sène, B. The Russo-Ukrainian war and financial markets: The role of dependence on Russian commodities. *Financ. Res. Lett.* **2022**, *50*, 103194. [CrossRef]
28. Szafranek, K.; Papież, M.; Rubaszek, M.; Śmiech, S. How immune is the connectedness of European natural gas markets to exceptional shocks? *Resour. Policy* **2023**, *85*, 103917. [CrossRef]
29. Zhou, E.; Wang, X. Dynamics of systemic risk in European gas and oil markets under the Russia-Ukraine conflict: A quantile regression neural network approach. *Energy Rep.* **2023**, *9*, 3956–3966. [CrossRef]
30. European Commission. REPowerEU. Available online: https://commission.europa.eu/strategy-and-policy/priorities-2019-2024/european-green-deal/repowereu-affordable-secure-and-sustainable-energy-europe_it (accessed on 15 May 2020).
31. Lamioni, R.; Bronzoni, C.; Folli, M.; Tognotti, L.; Galletti, C. Impact of H₂-enriched natural gas on pollutant emissions from domestic condensing boilers: Numerical simulations of the combustion chamber. *Int. J. Hydrogen Energy* **2023**, *48*, 19686–19699. [CrossRef]
32. de Miranda, P.E.V. Hydrogen Energy: Sustainable and Perennial. In *Science and Engineering of Hydrogen-Based Energy Technologies*; Elsevier: Amsterdam, The Netherlands, 2019; pp. 1–38.
33. Calise, F.; Cappiello, F.L.; Vicidomini, M. Chapter 9—Applications of Solar PV Systems in Hydrogen Production. In *Photovoltaic Solar Energy Conversion*; Gorjian, S., Shukla, A., Eds.; Academic Press: Cambridge, MA, USA, 2020; pp. 275–312. [CrossRef]

34. Harichandan, S.; Kar, S.K.; Bansal, R.; Mishra, S.K. Achieving sustainable development goals through adoption of hydrogen fuel cell vehicles in India: An empirical analysis. *Int. J. Hydrogen Energy* **2023**, *48*, 4845–4859. [[CrossRef](#)]
35. Ahmad, M.Z.; Ahmad, S.H.; Chen, R.S.; Ismail, A.F.; Hazan, R.; Baharuddin, N.A. Review on recent advancement in cathode material for lower and intermediate temperature solid oxide fuel cells application. *Int. J. Hydrogen Energy* **2022**, *47*, 1103–1120. [[CrossRef](#)]
36. Mehr, A.; Lanzini, A.; Santarelli, M.; Rosen, M.A. Polygeneration systems based on high temperature fuel cell (MCFC and SOFC) technology: System design, fuel types, modeling and analysis approaches. *Energy* **2021**, *228*, 120613. [[CrossRef](#)]
37. Peters, R.; Deja, R.; Engelbracht, M.; Frank, M.; Nguyen, V.N.; Blum, L.; Stolten, D. Efficiency analysis of a hydrogen-fueled solid oxide fuel cell system with anode off-gas recirculation. *J. Power Sources* **2016**, *328*, 105–113. [[CrossRef](#)]
38. Calise, F.; Cappiello, F.L.; Cimmino, L.; Vicidomini, M. Dynamic simulation modelling of reversible solid oxide fuel cells for energy storage purpose. *Energy* **2022**, *260*, 124893. [[CrossRef](#)]
39. Sun, L.; Wang, X.; Hua, Q.; Lee, K.Y. Energy scheduling of a fuel cell based residential cogeneration system using stochastic dynamic programming. *Process Saf. Environ. Prot.* **2023**, *175*, 272–279. [[CrossRef](#)]
40. Bhogilla, S.; Pandoh, A.; Singh, U.R. Cogeneration system combining reversible PEM fuel cell, and metal hydride hydrogen storage enabling renewable energy storage: Thermodynamic performance assessment. *Int. J. Hydrogen Energy* **2024**, *52*, 1147–1155. [[CrossRef](#)]
41. Tariq, A.H. Optimal sizing of photovoltaic/fuel cell-based energy system with autonomous oxygen production for hospitals in four climatic zones of Pakistan: An economic-energy-environmental feasibility analysis. *Renew. Energy Focus* **2023**, *47*, 100494. [[CrossRef](#)]
42. Isa, N.M.; Das, H.S.; Tan, C.W.; Yatim, A.H.M.; Lau, K.Y. A techno-economic assessment of a combined heat and power photovoltaic/fuel cell/battery energy system in Malaysia hospital. *Energy* **2016**, *112*, 75–90. [[CrossRef](#)]
43. Zhang, M.; Chen, X.; Chen, Y.; Jiang, S.; Shen, B. Combined cooling, heating, power and oxygen for hospital buildings employing photovoltaic power and liquefied methane. *Energy Rep.* **2022**, *8*, 815–821. [[CrossRef](#)]
44. Sleiti, A.K.; Al-Ammari, W.A.; Arshad, R.; El Mekki, T. Energetic, economic, and environmental analysis of solid oxide fuel cell-based combined cooling, heating, and power system for cancer care hospital. *Build. Simul.* **2022**, *15*, 1437–1454. [[CrossRef](#)]
45. Ghimire, R.; Niroula, S.; Pandey, B.; Subedi, A.; Thapa, B.S. Techno-economic assessment of fuel cell-based power backup system as an alternative to diesel generators in Nepal: A case study for hospital applications. *Int. J. Hydrogen Energy* **2024**, *56*, 289–301. [[CrossRef](#)]
46. Calise, F.; Cappiello, F.L.; Cimmino, L.; Dentice d’Accadia, M.; Vicidomini, M. Renewable smart energy network: A thermoeconomic comparison between conventional lithium-ion batteries and reversible solid oxide fuel cells. *Renew. Energy* **2023**, *214*, 74–95. [[CrossRef](#)]
47. Buonomano, A.; Palombo, A. Building energy performance analysis by an in-house developed dynamic simulation code: An investigation for different case studies. *Appl. Energy* **2014**, *113*, 788–807. [[CrossRef](#)]
48. Buonomano, A.; Calise, F.; Ferruzzi, G. Thermoeconomic analysis of storage systems for solar heating and cooling systems: A comparison between variable-volume and fixed-volume tanks. *Energy* **2013**, *59*, 600–616. [[CrossRef](#)]
49. Cui, Z.; Kang, L.; Li, L.; Wang, L.; Wang, K. A hybrid neural network model with improved input for state of charge estimation of lithium-ion battery at low temperatures. *Renew. Energy* **2022**, *198*, 1328–1340. [[CrossRef](#)]
50. Rashad, M.; Żabnieńska-Góra, A.; Norman, L.; Jouhara, H. Analysis of energy demand in a residential building using TRNSYS. *Energy* **2022**, *254*, 124357. [[CrossRef](#)]
51. Sornek, K.; Wiercioch, J.; Kurczyna, D.; Figaj, R.; Wójcik, B.; Borowicz, M.; Wielński, M. Development of a solar-powered small autonomous surface vehicle for environmental measurements. *Energy Convers. Manag.* **2022**, *267*, 115953. [[CrossRef](#)]
52. Calise, F.; Cappiello, F.L.; Dentice d’Accadia, M.; Petrakopoulou, F.; Vicidomini, M. A solar-driven 5th generation district heating and cooling network with ground-source heat pumps: A thermo-economic analysis. *Sustain. Cities Soc.* **2022**, *76*, 103438. [[CrossRef](#)]
53. Calise, F.; Cappiello, F.L.; Dentice d’Accadia, M.; Vicidomini, M. A novel smart energy network paradigm integrating combined heat and power, photovoltaic and electric vehicles. *Energy Convers. Manag.* **2022**, *260*, 115599. [[CrossRef](#)]
54. Karacavus, B.; Aydın, K. Hydrogen production and storage analysis of a system by using TRNSYS. *Int. J. Hydrogen Energy* **2020**, *45*, 34608–34619. [[CrossRef](#)]
55. Jani, D.B. Chapter 4—Performance Assessment of Solar Powered Hybrid Solid Desiccant and Dehumidification Integrated Thermally Cooling System Using TRNSYS. In *Advances in Clean Energy Technologies*; Azad, A.K., Ed.; Academic Press: Cambridge, MA, USA, 2021; pp. 171–203. [[CrossRef](#)]
56. Ma, Y.; Xi, J.; Cai, J.; Gu, Z. TRNSYS simulation study of the operational energy characteristics of a hot water supply system for the integrated design of solar coupled air source heat pumps. *Chemosphere* **2023**, *338*, 139453. [[CrossRef](#)] [[PubMed](#)]
57. Buonomano, A.; Calise, F.; Ferruzzi, G.; Palombo, A. Dynamic energy performance analysis: Case study for energy efficiency retrofits of hospital buildings. *Energy* **2014**, *78*, 555–572. [[CrossRef](#)]
58. Voit, P.; Lechner, T.; Schuler, M. Common EC validation procedure for dynamic building simulation programs—application with TRNSYS. In *Proceedings of the Conference of International Simulation Societies, Zurich, Switzerland, 22–25 August 1994*.
59. Guercio, A.; Curto, D.; Franzitta, V.; Frascati, M.; Milone, D.; Martorana, P.; Mantegna, M. Energy Analyses and Optimization Proposals for Hotels in Sicily: A Case Study. *Sustainability* **2024**, *16*, 146. [[CrossRef](#)]

60. Palaić, D.; Štajduhar, I.; Ljubic, S.; Wolf, I. Development, Calibration, and Validation of a Simulation Model for Indoor Temperature Prediction and HVAC System Fault Detection. *Buildings* **2023**, *13*, 1388. [CrossRef]
61. Rezaei, E.; Dzuryk, S. Techno-economic comparison of reverse water gas shift reaction to steam and dry methane reforming reactions for syngas production. *Chem. Eng. Res. Des.* **2019**, *144*, 354–369. [CrossRef]
62. Kumar, R.; Kumar, A.; Pal, A. Simulation modelling of hydrogen production from steam reforming of methane and biogas. *Fuel* **2024**, *362*, 130742. [CrossRef]
63. Perry, R.H.; Green, D.W.; Maloney, J.O. (Eds.) *Perry's Chemical Engineers' Handbook*, 6th ed.; McGraw-Hill: New York, NY, USA, 1984.
64. Maggio, G.; Squadrito, G.; Nicita, A. Hydrogen and medical oxygen by renewable energy based electrolysis: A green and economically viable route. *Appl. Energy* **2022**, *306*, 117993. [CrossRef]
65. Nicita, A.; Maggio, G.; Andaloro, A.P.F.; Squadrito, G. Green hydrogen as feedstock: Financial analysis of a photovoltaic-powered electrolysis plant. *Int. J. Hydrogen Energy* **2020**, *45*, 11395–11408. [CrossRef]
66. Koumi Ngoh, S.; Bakehe, J.F.; Edouma Fils, P. Green electricity and medical electrolytic oxygen from solar energy—A sustainable solution for rural hospitals. *Sci. Afr.* **2022**, *17*, e01389. [CrossRef]
67. Squadrito, G.; Nicita, A.; Maggio, G. A size-dependent financial evaluation of green hydrogen-oxygen co-production. *Renew. Energy* **2021**, *163*, 2165–2177. [CrossRef]
68. Katebah, M.; Al-Rawashdeh, M.m.; Linke, P. Analysis of hydrogen production costs in Steam-Methane Reforming considering integration with electrolysis and CO₂ capture. *Clean. Eng. Technol.* **2022**, *10*, 100552. [CrossRef]
69. Böhm, H.; Zauner, A.; Rosenfeld, D.C.; Tichler, R. Projecting cost development for future large-scale power-to-gas implementations by scaling effects. *Appl. Energy* **2020**, *264*, 114780. [CrossRef]
70. Carr, S.; Premier, G.C.; Guwy, A.J.; Dinsdale, R.M.; Maddy, J. Hydrogen storage and demand to increase wind power onto electricity distribution networks. *Int. J. Hydrogen Energy* **2014**, *39*, 10195–10207. [CrossRef]
71. Luyben, W.L. Capital cost of compressors for conceptual design. *Chem. Eng. Process.-Process Intensif.* **2018**, *126*, 206–209. [CrossRef]
72. Calise, F.; Cappiello, F.L.; Dentice d'Accadia, M.; Vicidomini, M. Smart grid energy district based on the integration of electric vehicles and combined heat and power generation. *Energy Convers. Manag.* **2021**, *234*, 113932. [CrossRef]
73. Calise, F.; Dentice d'Accadia, M.; Piacentino, A. A novel solar trigeneration system integrating PVT (photovoltaic/thermal collectors) and SW (seawater) desalination: Dynamic simulation and economic assessment. *Energy* **2014**, *67*, 129–148. [CrossRef]
74. Musharavati, F.; Khanmohammadi, S. Performance improvement of a heat recovery system combined with fuel cell and thermoelectric generator: 4E analysis. *Int. J. Hydrogen Energy* **2021**, *47*, 26701–26714. [CrossRef]
75. Nadir, M.; Ghenaïet, A.; Carcasci, C. Thermo-economic optimization of heat recovery steam generator for a range of gas turbine exhaust temperatures. *Appl. Therm. Eng.* **2016**, *106*, 811–826. [CrossRef]
76. Zhai, H.; Rubin, E.S. Performance and cost of wet and dry cooling systems for pulverized coal power plants with and without carbon capture and storage. *Energy Policy* **2010**, *38*, 5653–5660. [CrossRef]
77. Available online: <https://eshop.czechminibreweries.com/> (accessed on 15 May 2020).
78. Jenbacher-Werke. 2019. Available online: <https://www.innio.com/en/products/jenbacher> (accessed on 15 May 2020).
79. Kupecki, J.; Motylinski, K.; Jagielski, S.; Wierzbicki, M.; Brouwer, J.; Naumovich, Y.; Skrzypkiewicz, M. Energy analysis of a 10 kW-class power-to-gas system based on a solid oxide electrolyzer (SOE). *Energy Convers. Manag.* **2019**, *199*, 111934. [CrossRef]
80. Sanz-Bermejo, J.; Muñoz-Antón, J.; Gonzalez-Aguilar, J.; Romero, M. Part load operation of a solid oxide electrolysis system for integration with renewable energy sources. *Int. J. Hydrogen Energy* **2015**, *40*, 8291–8303. [CrossRef]
81. Stempien, J.P.; Sun, Q.; Chan, S.H. Solid Oxide Electrolyzer Cell Modeling: A Review. *J. Power Technol.* **2013**, *93*, 216–246.

Disclaimer/Publisher's Note: The statements, opinions and data contained in all publications are solely those of the individual author(s) and contributor(s) and not of MDPI and/or the editor(s). MDPI and/or the editor(s) disclaim responsibility for any injury to people or property resulting from any ideas, methods, instructions or products referred to in the content.